

Quantitative Kinetic Analysis in a Microfluidic Device Using Frequency-Domain Fluorescence Lifetime Imaging

Sinéad M. Matthews,[†] Alan D. Elder,[†] Kamran Yunus,[†] Clemens F. Kaminski,[†] Colin M. Brennan,[‡] and Adrian C. Fisher^{*†}

Department of Chemical Engineering, University of Cambridge, New Museums Site, Pembroke Street, Cambridge, CB2 3RA, UK, and Huddersfield Manufacturing Centre, Syngenta Ltd., P.O. Box A38, Leeds Road, Huddersfield, HD2 1FF, UK

A novel microfluidic approach for the quantification of reaction kinetics is presented. A three-dimensional finite difference numerical simulation was developed in order to extract quantitative kinetic information from fluorescence lifetime imaging experimental data. This approach was first utilized for the study of a fluorescence quenching reaction within a microchannel; the lifetime of a fluorophore was used to map the diffusion of a quencher across the microchannel. The approach was then applied to a more complex chemical reaction between a fluorescent amine and an acid chloride, via numerical simulation the bimolecular rate constant for this reaction was obtained.

The potential advantages of using a microfluidic approach for the study of a number of physical processes such as diffusion,¹ phase transfer,² protein folding,³ and reaction kinetics⁴ have been well documented. The high transport rates within microchannels enables the study of rapid kinetic processes within liquid media. A range of different in situ analytical techniques have been developed for the quantification of kinetic and fluid dynamic processes within microfluidic devices including; confocal fluorescence microscopy,⁵ magnetic resonance imaging,⁶ optical coherence tomography,⁷ fluorescence correlation spectroscopy,⁸ and fluorescent lifetime imaging microscopy (FLIM).⁹

In this article, we describe the application of fluorescence lifetime imaging for the quantification of reaction processes occurring within a microfluidic device. The lifetime is sensitive to a molecule's interactions with its surroundings and can be used to provide quantitative information on the local environment such as pH changes,¹⁰ diffusional mobility,¹¹ conformational changes,¹² and quenching.¹³ This sensitivity enables species that cannot be resolved using spectral techniques to be discriminated using their lifetimes.¹⁴ Within a microfluidic device, it is relatively simple to control conditions such as the pH,¹⁵ ion concentration,¹⁶ and temperature,¹⁷ thus making FLIM a powerful analytical technique. Previous studies have demonstrated the use of FLIM for the quantification of processes such as molecular mixing and diffusion within microchannels.^{9,18} Recently, we reported the quantitative analysis of the quenching of Rhodamine 6G by potassium iodide using FLIM.^{19,20}

In order to extract quantitative mechanistic and kinetic parameters from spectroscopic data, it is necessary to simulate the combined mass transport and reaction kinetic processes within a specific device. Recently we have demonstrated the quantification of combined fluid dynamic and mass transport problems within microfluidic devices where electrochemical analysis is performed.^{21,22} While direct analytical solution of the governing

* To whom correspondence should be addressed; E-mail: acf42@cam.ac.uk. Tel.: +44 (0) 1223 763996. Fax: +44 (0) 1223 767407.

[†] University of Cambridge.

[‡] Syngenta Ltd.

- (1) Kamholz, A. E.; Schilling, E. A.; Yager, P. *Biophys. J.* **2001**, *80*, 1967–1972.
- (2) Kim, H. B.; Ueno, K.; Chiba, M.; Kogi, O.; Kitamura, N. *Anal. Sci.* **2000**, *16*, 871–876.
- (3) Bilsel, O.; Kayatekin, C.; Wallace, L. A.; Matthews, C. R. *Rev. Sci. Instrum.* **2005**, *76*, 014302.
- (4) Cao, C.; Xia, G.; Holladay, J.; Jones, E.; Wang, Y. *Appl. Catal., A* **2004**, *262*, 19–29.
- (5) Ismagilov, R. F.; Stroock, A. D.; Kenis, P. J. A.; Whitesides, G.; Stone, H. A. *Appl. Phys. Lett.* **2000**, *76*, 2376–2378.
- (6) Wensink, H.; Bebito-Lopez, F.; Hermes, D. C.; Verboom, W.; Gardeniers, H. J. G. E.; Reinhoudt, D. N.; van den Berg, A. *Lab Chip* **2005**, *5*, 281–284.
- (7) Ahn, Y. C.; Jung, W.; Zhang, J.; Chen, Z. *Opt. Express* **2005**, *13*, 8164–8171.
- (8) Kuricheti, K. K.; Buschnmann, V.; Brister, P.; Weston, K. D. In *Microfluidics, BioMEMS, and Medical Microsystems II*; Woias, P., Papautsky, I., Eds.; SPIE Proceedings Series 5345; SPIE: Bellingham, WA, 2003; pp 194–205.
- (9) Magennis, S. W.; Graham, E. M.; Jones, A. C. *Agnew. Chem., Int. Ed.* **2005**, *44*, 6512–6516.
- (10) Lin, H. J.; Herman, P.; Lakowicz, J. R. *Cytometry, Part A* **2003**, *52* (2), 77–89.
- (11) Clayton, A. H.; Hanley, Q. S.; Arndt-Jovin, D. J. *Biophys. J.* **2002**, *83* (3), 1631–1649.
- (12) Calleja, V.; Ameer-Beg, S. M.; Vojnovic, B. *Biochem. J.* **2003**, *372*, 33–40.
- (13) Szmajcinski, H.; Lakowicz, J. R. *Sens. Actuator, B: Chem.* **1995**, *29* (1–3), 16–24.
- (14) Dowling, K.; Dayel, M. J.; Lever, M. J.; French, P. M. W.; Hares, J. D.; Dymoke-Bradshaw, A. K. L. *Opt. Lett.* **1998**, *23*, 810–812.
- (15) Cabrera, C. R.; Finlayson, B.; Yager, P. *Anal. Chem.* **2001**, *73*, 658–666.
- (16) Yang, M.; Yang, J.; Li, C. W.; Zhao, J. *Lab Chip* **2002**, *2*, 158–163.
- (17) Mao, H.; Yang, T.; Cremer, P. S. *J. Am. Chem. Soc.* **2002**, *124*(16), 4432–4435.
- (18) Benninger, R. K. P.; Hofmann, O.; McGinty, J.; Requejo-Isidro, J.; Munro, I.; Neil, M. A. A.; deMello, A. J.; French, P. M. W. *Opt. Express* **2005**, *13*, 6275–6285.
- (19) Elder, A. D.; Matthews, S. M.; Swartling, J.; Yunus, K.; Frank, J. H.; Brennan, C. M.; Fisher, A. C.; Kaminski, C. F. *Opt. Express* **2006**, *14*, 5456–5467.
- (20) Elder, A. D.; Frank, J. H.; Swartling, J.; Dai, X.; Kaminski, C. F. *J. Microsc.* In press.
- (21) Matthews, S. M.; Du, G. Q.; Fisher, A. C. *J. Solid State Electrochem.* **2006**, *10* 817–826.

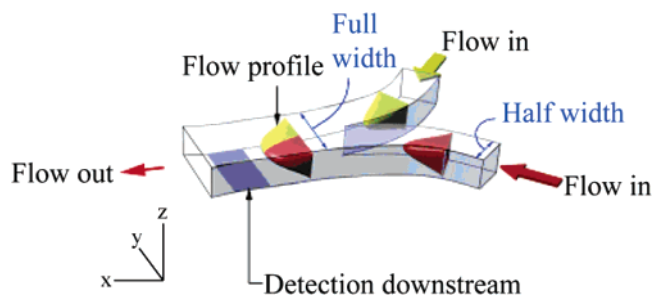


Figure 1. Schematic of a microreactor.

equations is possible for simple geometries,²³ it is common to resort to numerical strategies for most practical applications and there are a number of different approaches taken in the literature. Finite difference (FD) techniques have been applied to a number of microfluidic devices including electrolysis reactions and fluid flow.²⁴ The relatively simple modification of boundary conditions using FD techniques to incorporate reaction between species has previously been reported for hydrodynamic studies.²⁵ Where cell geometries are more irregular, techniques such finite element,^{26,27} boundary element,^{28,29} and lattice Boltzmann^{30,31} have been utilized. The simulation of chemical reactions within microfluidic devices has also been reported using two-dimensional models of high aspect ratio devices with an assumption of uniform velocity profiles across the width of the microchannel.^{32,33}

In this article, the well-defined structural nature of the micro-fabricated devices allows the FD approach to be employed without compromising accuracy. This was achieved by the development of a three-dimensional FD model to quantify the mass transport and reaction processes occurring within the microchannels. The numerical models allow the prediction of concentration and lifetime distributions within a microfluidic device for potential candidate mechanisms and the quantification of the experimentally measured rate constants. The kinetic parameters of two experimental systems were interrogated using this approach, the quenching of Rhodamine 6G by potassium iodide and the chemical reaction between 2-aminoacridone and benzoyl chloride.

THEORY

In this section, the theoretical treatment of a second-order reaction in the microreactor shown in Figure 1 is described. In order to develop the numerical simulation, the concentration

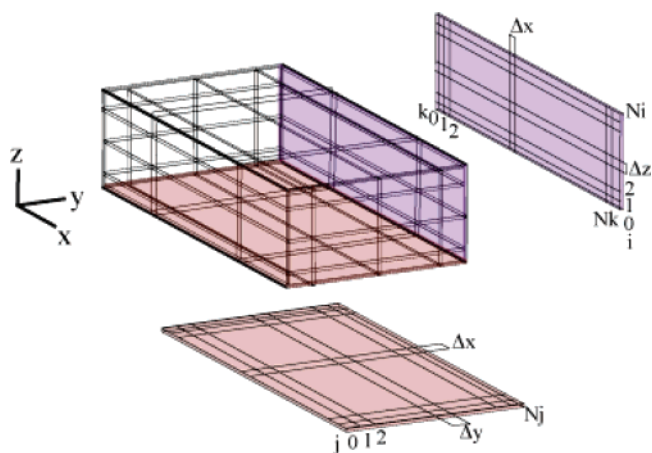


Figure 2. Finite difference grid.

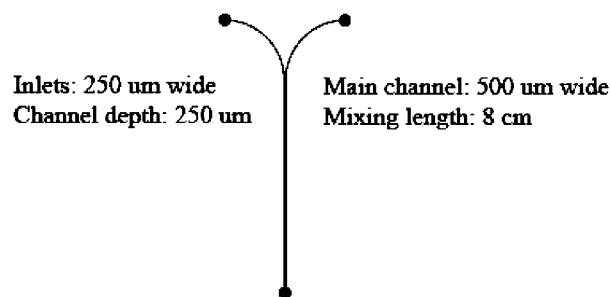


Figure 3. Design of microreactor.

distributions of two species in solution due to mass transport and the relevant chemical kinetics need to be formulated. The relevant convective diffusion equation for species A and B is given below.

$$\frac{\partial[A]}{\partial t} = D_A \frac{\partial^2[A]}{\partial x^2} + D_A \frac{\partial^2[A]}{\partial y^2} + D_A \frac{\partial^2[A]}{\partial z^2} - v_x \frac{\partial[A]}{\partial x} \pm k[A]^n[B]^m \quad (1)$$

$$\frac{\partial[B]}{\partial t} = D_B \frac{\partial^2[B]}{\partial x^2} + D_B \frac{\partial^2[B]}{\partial y^2} + D_B \frac{\partial^2[B]}{\partial z^2} - v_x \frac{\partial[B]}{\partial x} \pm k[A]^n[B]^m \quad (2)$$

where D_A and D_B are the diffusion coefficients of species A and B respectively, v_x is the velocity in the x direction, k is the rate constant, n and m are the order of reaction with respect to species A and B, and the coordinates x , y , and z are defined in Figure 1. The three-dimensional velocity profile can be solved analytically for laminar flow,³⁴ provided the flow has become fully developed.

$$v_x = \frac{16\beta^2}{\pi^4} \sum_{n(\text{odd})} \sum_{m(\text{odd})} \frac{\sin\left(\frac{n\pi\xi}{a}\right) \sin\left(\frac{m\pi\eta}{b}\right)}{nm(\beta^2 n^2 + m^2)} \quad (3)$$

where a is the height (h_2), b is the width (d_a), β is the height/width ratio, ξ is the position along the y -axis, and η is the position along the z -axis. The length of the channel is denoted as x_1 .

- (22) Sullivan, S. P.; Johns, M. L.; Matthews, S. M.; Fisher, A. C. *Electrochem. Commun.* **2005**, *7*, 1323–1328.
- (23) Kamholz, A. E.; Weigl, B. H.; Finlayson, B. A.; Yager, P. *Anal. Chem.* **1999**, *71*, 5340–5347.
- (24) Koo, J.; Kleinstreuer, C. *J. Microchem. Microeng.* **2003**, *13*, 568–579.
- (25) Compton, R. G.; Pilkington, M. B. G.; Stearn, G. M. *J. Chem. Soc., Faraday Trans. 1* **1988**, *84*, 2155–2171.
- (26) Menegeaud, V.; Josserand, J.; Girault, H. H. *Anal. Chem.* **2002**, *74*, 4279–4286.
- (27) Beskok, A.; Warburton, T. C. *J. Comput. Phys.* **2001**, *174*, 492–509.
- (28) Gaver, D. P.; Kute, S. M. *Biophys. J.* **1998**, *75*, 721–733.
- (29) Qui, F. L.; Fisher, A. C. *Electrochem. Commun.* **2003**, *5*, 87–93.
- (30) Nie, X.; Doolen, G. D.; Chen, S. *J. Stat. Phys.* **2002**, *107* (1–2), 279–289.
- (31) Sullivan, S. P.; Akpa, B. S.; Matthews, S. M.; Fisher, A. C.; Gladden, L. F.; Johns, M. L. *Sens. Actuators. B.* In press.
- (32) Baroud, C.; Menetrier, L.; Okkels, F.; Tabeling, P. *International conference on miniaturised chemical and biochemical analysis systems*; 2003; Vol. 7, pp 943–946.
- (33) Salmon, J.-B.; Dubrocq, C.; Tabeling, P.; Charier, S.; Alcor, D.; Jullien, L.; Ferrage, F. *Anal. Chem.* **2005**, *77*, 3417–3424.

- (34) Spiga, M.; Morini, G. L. *Int. Commun. Heat Mass Trans.* **1994**, *21*, 469.

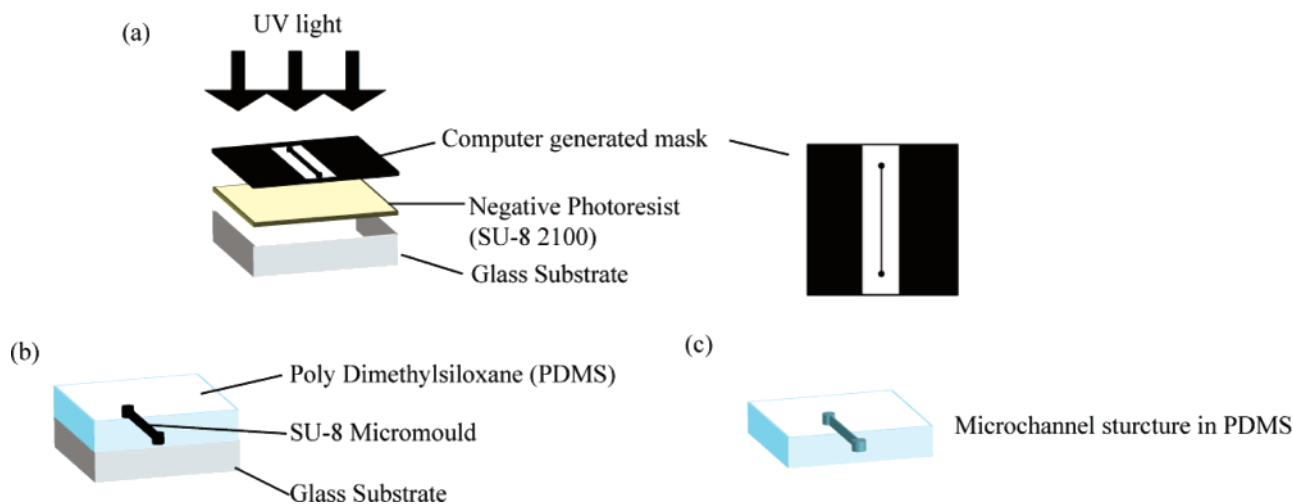


Figure 4. Schematic of microfabrication process.

To determine the concentration distributions of species A and B, the following boundary conditions were applied.

The initial boundary conditions are defined so that species A occupies half of the channel width and species B occupies the other half:

$t = 0$

$$\left[\begin{array}{l} 1 < x < x_1 \quad 1 < y < \frac{d_d}{2} \quad 1 < z < h_2 \quad [A] = 1, [B] = 0 \\ 1 < x < x_1 \quad \frac{d_d}{2} < y < d_d \quad 1 < z < h_2 \quad [A] = 0, [B] = 1 \end{array} \right]$$

At $t > 0$

$$\left[\begin{array}{l} x = 1 \quad 1 < y < \frac{d_d}{2} \quad 1 < z < h_2 \quad [A] = 1, [B] = 0 \\ x = 1 \quad \frac{d_d}{2} < y < d_d \quad 1 < z < h_2 \quad [A] = 0, [B] = 1 \\ 1 < x < x_1 \quad 1 < y < d_d \quad z = 0 \quad \frac{\partial[A]}{\partial z} = 0, \frac{\partial[B]}{\partial z} = 0 \\ 1 < x < x_1 \quad 1 < y < d_d \quad z = h_2 \quad \frac{\partial[A]}{\partial z} = 0, \frac{\partial[B]}{\partial z} = 0 \\ 1 < x < x_1 \quad y = 0 \quad 1 < z < h_2 \quad \frac{\partial[A]}{\partial y} = 0, \frac{\partial[B]}{\partial y} = 0 \\ 1 < x < x_1 \quad y = d_d \quad 1 < z < h_2 \quad \frac{\partial[A]}{\partial y} = 0, \frac{\partial[B]}{\partial y} = 0 \end{array} \right]$$

Equations 1 and 2 were solved using the Backward Implicit algorithm, which has been used for electrochemical simulations of both macro- and microchannels.^{21,25} The technique is applied by using a finite difference grid, shown in Figure 2, over the channel in the x , y , and z directions with increments of Δx , Δy , and Δz , respectively. The grid parameters were increased until further increases produced no significant difference in the calculated concentrations using a procedure identical to that highlighted previously.²⁵ All programs were written in f77 gcc version 3.3.3 and run on Linux Fedora Core 2.6.

During the development of this program, it was demonstrated that lateral diffusion (along the z -axis) was insignificant in typical experimental conditions. Therefore, diffusion in the z direction was omitted from the calculation for simplicity as this resulted in a more rapid solution with no observed loss of accuracy.

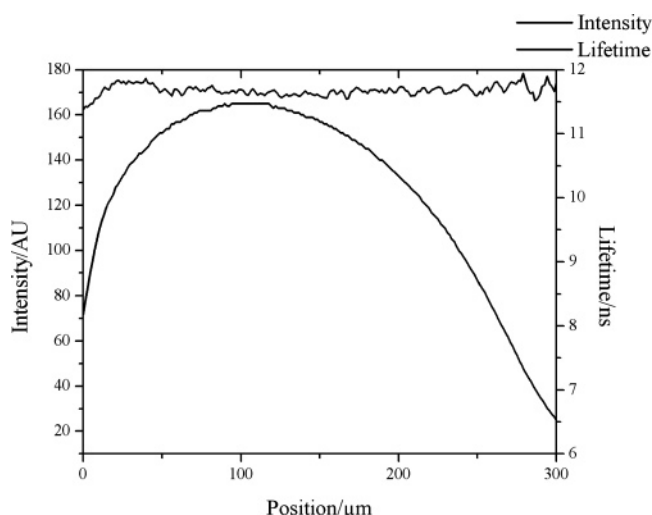


Figure 5. Intensity and lifetime profiles across the width of the microchannel for the blank experiment.

EXPERIMENTAL PROCEDURES

Channel Fabrication. The microchannel design developed for both the quenching and chemical reaction systems is shown in Figure 3. Previous work had demonstrated that poly(dimethylsiloxane) (PDMS) produced no significant background signal at the desired wavelengths.¹⁹ PDMS microchannels are prepared by the photolithographic fabrication of a micromold, which is then immersed in PDMS elastomer and allowed to cure.

The mask was designed using a technical drawing package and printed (Circuit Graphics, Chelmsford, UK) to produce a high-resolution acetate mask. A film of SU-8 2100 (Microchem) of ~ 250 - μm thickness, was spun onto a glass wafer (Karl Suss Delta 10TT). This was then prebaked at 65 and 95 $^{\circ}\text{C}$ for 12 min and 1 h, respectively, and exposed to UV light (340 nm; Karl Suss MJB3 Mask Aligner) through the acetate mask. After postbaking at 65 and 95 $^{\circ}\text{C}$ for 1 and 15 min, respectively, the wafer was then soaked in developer solution (EC Solvent, Microchem) to reveal the micromold. PDMS (Sylgard 184, Dow Corning) was then poured over the master and allowed to cure overnight. Once set, the PDMS channel was peeled away from the master (which could be reused); glass inlets and outlets were inserted and secured

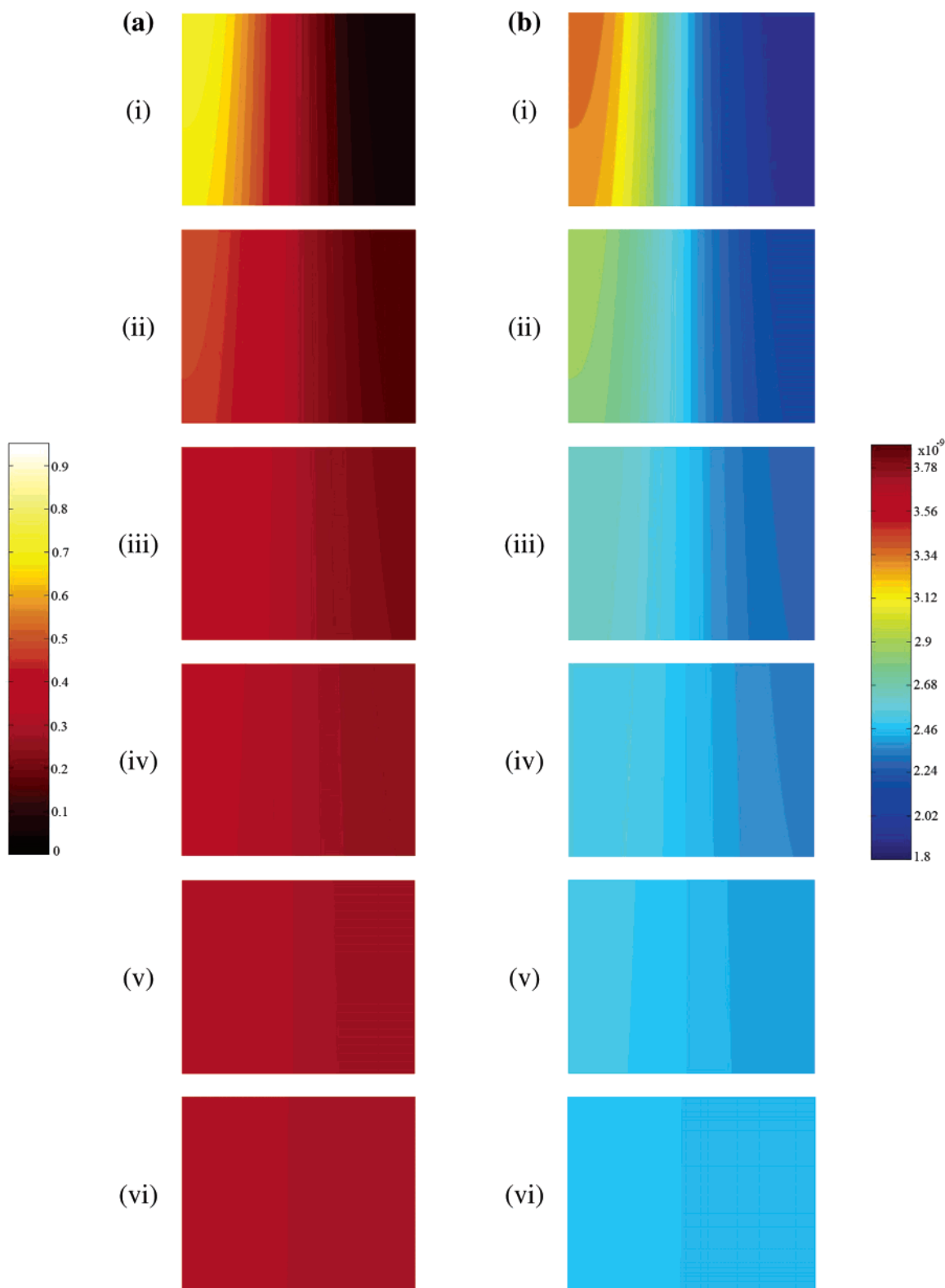


Figure 6. (a) Iodide ion concentration map and (b) lifetime map at (i) 1 cm after inlet, (ii) 2 cm after inlet, (iii) 3 cm after inlet, (iv) 4 cm after inlet, (v) 5 cm after inlet, and (vi) 6 cm after inlet.

using an epoxy resin (Araldite) and sealed to a clean glass wafer using the natural adhesiveness of PDMS. A schematic of the microfabrication procedure is shown in Figure 4.

FLIM Setup. The experimental data were obtained using an Olympus IX70 inverted microscope (Olympus UK Ltd., Southall, UK) with the LIFA FLIM system (Lambert Instruments, Leut-

ingewold, The Netherlands). LED excitation was provided by a 3-W LED centered at 473 nm. The excitation and emission lights were filtered using a 470–490-nm bandpass filter, a 500-nm dichroic mirror, and a 515-nm long-pass filter, respectively. The images were obtained using an ICCD whose gain was modulated at the same frequency as the LED excitation.

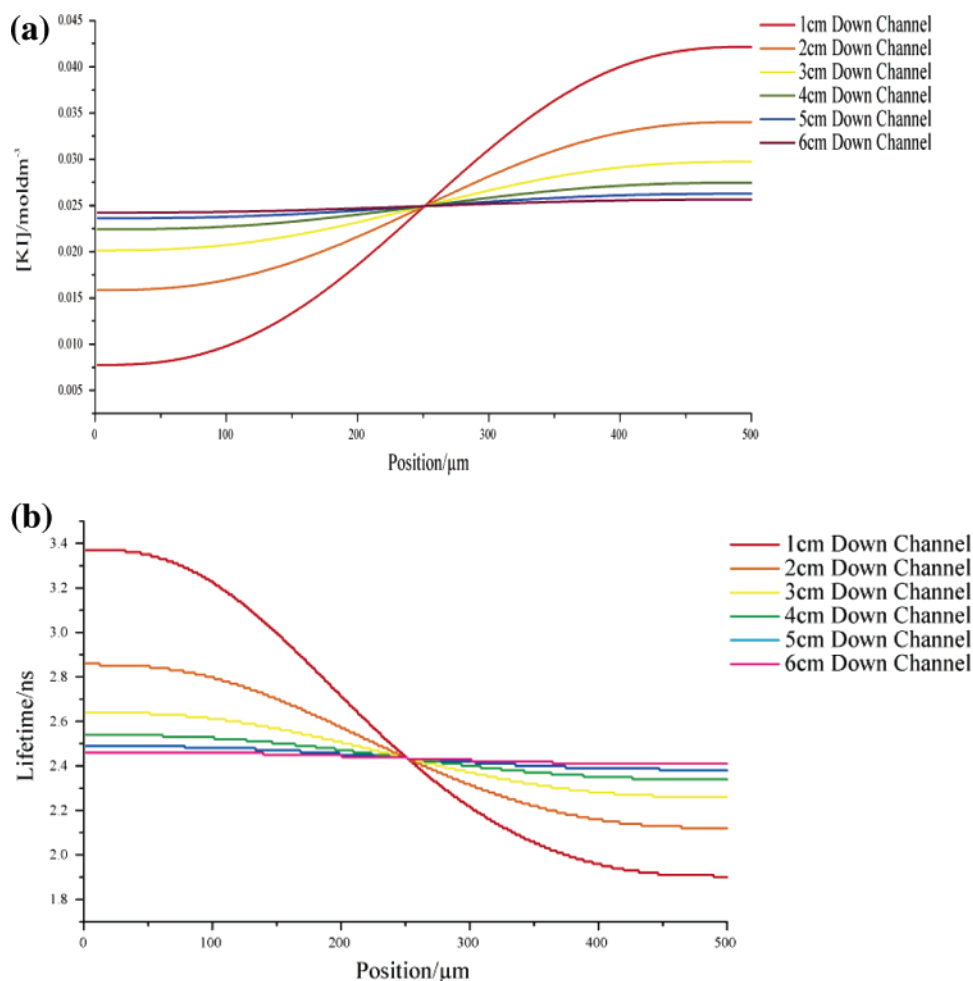


Figure 7. Simulated (a) iodide ion concentration (b) lifetime profiles across channel.

Flow to the microchannel was controlled using a syringe pump (Harvard Apparatus, PHD 2000); one inlet contained a 1×10^{-6} mol dm^{-3} solution of Rhodamine 6G with 0.05 mol dm^{-3} KI, the other inlet contained a 1×10^{-6} mol dm^{-3} solution of Rhodamine 6G with 0.05 mol dm^{-3} KCl (KCl was added to maintain the ionic strength of the solution). A series of fluorescence lifetime images were taken at five positions down the channel to monitor the diffusion of the iodide ion across the two streams. A total volume flow rate of $1.667 \times 10^{-4} \text{ cm}^3 \text{ s}^{-1}$ was identified, using the simulations described below, to ensure a uniform iodide ion concentration by the end of the observation region of the channel. The full details of this experimental procedure have been described previously.¹⁹

2-Aminoacridone (Fluka, 98%) was used as supplied; solutions were prepared in acetonitrile (Fisher, HPLC grade). While the optimum excitation wavelength for this compound is 425 nm, previous studies have demonstrated that it has a sufficiently broad tail in its excitation peak to be excited at higher wavelengths.³⁵ Benzoyl chloride (Aldrich, 99%) was used as supplied and diluted using acetonitrile. All acetonitrile was dried using 3-Å molecular sieves (Fluka) to prevent benzoyl chloride hydrolysis. A calibration procedure was performed, which demonstrated that the fluorescence lifetime varied linearly with the percentage reaction and

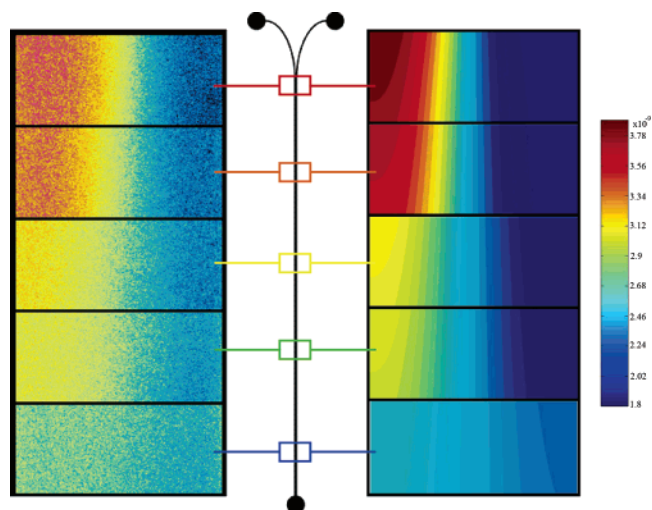


Figure 8. Experimental and simulated fluorescence lifetime maps for Rhodamine 6G quenching experiment.

that the fluorescence was not quenched by any species present in the channel.

Flow to the microchannel was delivered using gravity flow; the relative heights of the two reservoirs were adjusted to ensure equal flow rates at each inlet. One inlet contained a fluorescent 2-aminoacridone solution, and the other contained a non-fluores-

(35) Hill, E. K.; de Mello, A. J.; Birrell, H.; Charlwood, J.; Camilleri. *P. J. Chem. Soc., Perkin Trans. 2.* **1998**, 2337–2341.

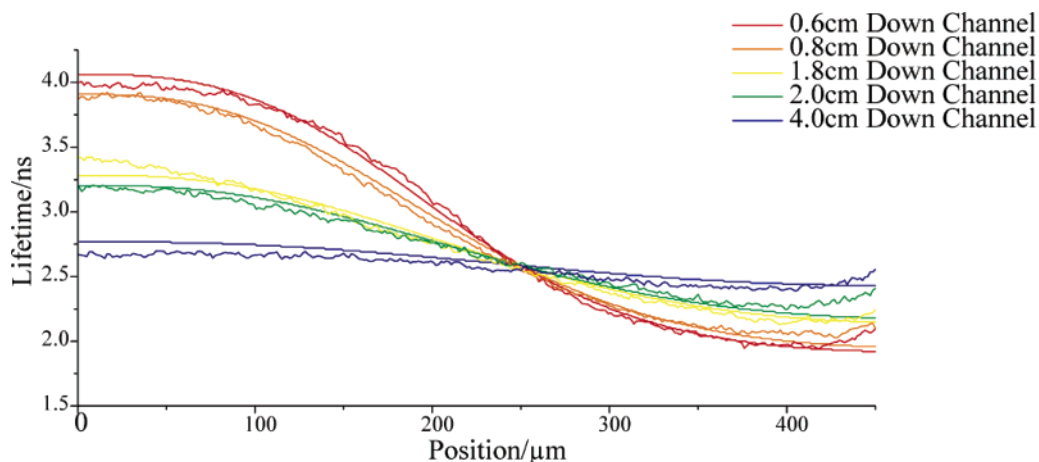


Figure 9. Average Rhodamine 6G lifetime profiles across the channel from different positions down the channel.

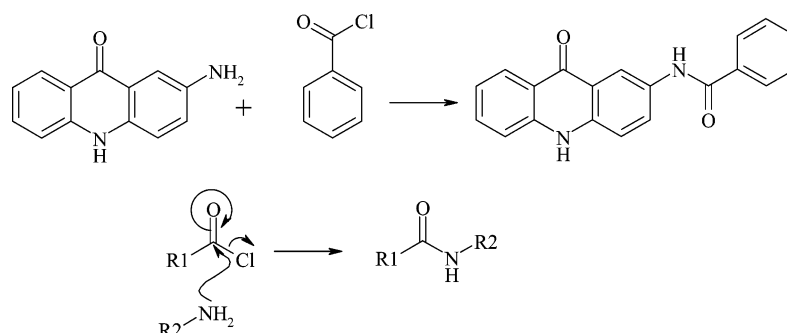


Figure 10. Reaction scheme and proposed mechanism.

cent benzoyl chloride solution. The fluorescence lifetime was measured at the end of the observation region of the channel, and the total volume flow rate was adjusted until a significant change in lifetime was observed across the width of the channel; this was measured at the outlet to be $0.003 \text{ cm}^3 \text{ s}^{-1}$. The fluorescence lifetime was then measured at six positions down the channel to monitor the evolution of the product concentration profile.

A blank experiment, where the non-fluorescent stream contained no benzoyl chloride, was also performed where both the fluorescent intensity and lifetime were recorded. The intensity and lifetime profiles across the microchannel are shown in Figure 5. This clearly demonstrates one of the key advantages for using FLIM as the lifetime remains uniform across the channel, whereas the intensity varies with position despite no reaction occurring. This blank experiment has also been used to estimate the experimental error of the fluorescence lifetime measurement. The lifetime profile for the blank measurement should be constant, and so by looking at the standard deviation in values across the profile, we can get an estimate for the error in individual profile points. The profile was averaged over the width of the channel and the standard deviation of this average calculated; this results in an error of less than $\pm 1\%$ in individual points in the lifetime profiles.

RESULTS AND DISCUSSION

Initial quantitative studies focused on the analysis of the fluorescence quenching of Rhodamine 6G by potassium iodide within a microchannel. Preliminary calculations were carried out for a variety of experimental conditions such as channel dimensions and flow rates in order to identify optimum reaction

conditions. The diffusion coefficients were set as follows: $D_{\text{R6G}} = 2.6 \times 10^{-6} \text{ cm}^2 \text{ s}^{-1}$,³⁵ and $D_{\text{I}^-} = 2.045 \times 10^{-5} \text{ cm}^2 \text{ s}^{-1}$.³⁶ The optimized parameters were as follows: $h_2 = 0.025 \text{ cm}$, $d_d = 0.05 \text{ cm}$, $x_1 = 6 \text{ cm}$, $v_f = 1.667 \times 10^{-5} \text{ cm}^3 \text{ s}^{-1}$, $N_K = 4000$, $N_j = 500$, and $N_i = 80$.

In order to correspond with the experimental procedure, the boundary conditions were applied so that Rhodamine 6G appeared in both inlet streams:

$$\left[\begin{array}{l} x = 1 \quad 1 < y < \frac{d_d}{2} \quad 1 < z < h_2 \quad [\text{I}^-] = 1, [\text{R6G}] = 1 \\ x = 1 \quad \frac{d_d}{2} < y < d_d \quad 1 < z < h_2 \quad [\text{I}^-] = 0, [\text{R6G}] = 1 \end{array} \right]$$

Lifetimes were recorded in wide-field imaging mode over a 2 mm length of channel. Consequently, the slices shown in Figure 6a have been calculated by integrating the simulated concentration over the height of the channel for a 2 mm sample region and then averaged. The corresponding lifetime may be calculated from the concentration distribution using the Stern–Volmer equation:

$$\frac{1}{\tau} = k_q[\text{Q}] + \frac{1}{\tau^0} \quad (4)$$

where τ^0 is the lifetime of the fluorophore in the absence of a quencher (4.08 ns for Rhodamine 6G³⁸), k_q is the bimolecular

(36) Xu, Y, *Science* **1997**, 275, 1106–1110.

(37) Lide, D. R., Ed. *Handbook of Chemistry and Physics*, 77th ed.; CRC Press: Boca Raton, FL, 1996.

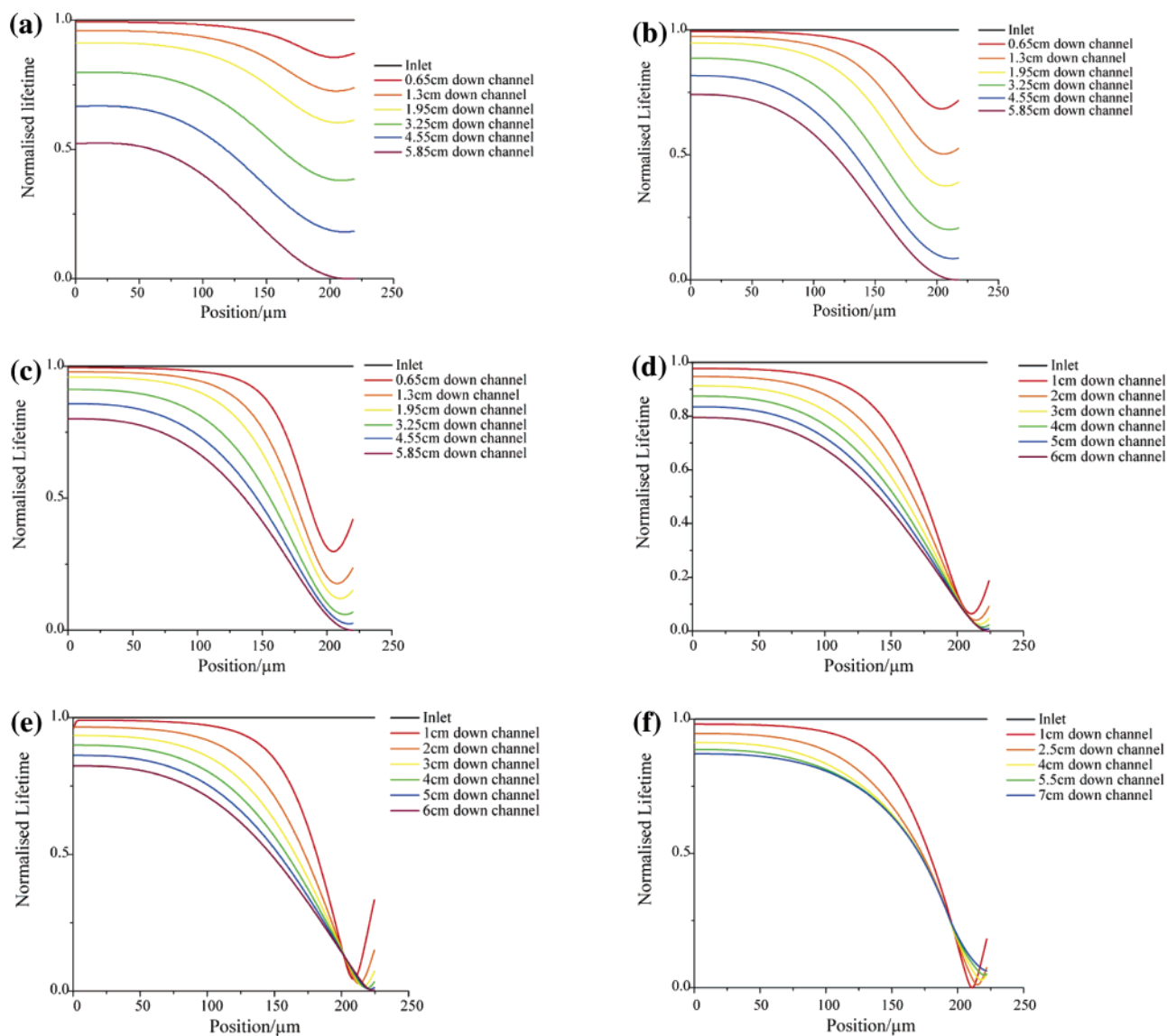


Figure 11. Simulated normalized lifetime profiles for the reaction between 2-aminoacridone and benzoyl chloride with a bimolecular constant of (a) 1×10^1 , (b) 1×10^2 , (c) 1×10^3 , (d) 1×10^4 , (e) 1×10^5 , and (f) $1 \times 10^6 \text{ dm}^3 \text{ mol}^{-1} \text{ s}^{-1}$.

quenching rate constant ($6.64 \times 10^9 \text{ dm}^3 \text{ mol}^{-1} \text{ s}^{-1}$),²⁰ and $[Q]$ is the quencher concentration.

Concentration and lifetime profiles across the channel were obtained by averaging the concentration/lifetime over the 2-mm imaging section in accordance with experimental procedures. The concentration and lifetime profiles for the positions used in Figure 6 are shown in Figure 7.

Initial experimental investigations were focused on the quenching of Rhodamine 6G by potassium iodide, which we have previously studied using FLIM.¹⁹ A $1 \times 10^{-6} \text{ mol dm}^{-3}$ solution of Rhodamine 6G was pumped through both inlets with one stream also containing 0.05 mol dm^{-3} potassium iodide, the resulting lifetime change was used to calculate the iodide ion concentration. Using the above numerical approach with an experimentally determined bimolecular quenching rate constant, the experimental data were compared to the simulated predictions for the Stern–Volmer model quenching. The comparisons of

experimental and simulated lifetime and concentration maps are shown in Figure 8, and Figure 9 shows the corresponding experimental and simulation lifetime profiles across the channel.

Figure 8 shows good agreement between the experimental and simulated lifetime maps for all positions down the channel. This confirms that the numerical model can be used to accurately predict the concentration distribution of a species within the microchannel. This comparison clearly demonstrates that averaging the lifetime over the height of the channel is a suitable analogy to the experimentally used wide-field imaging technique. The comparison between experimental and simulated lifetime profiles shown in Figure 9 further illustrates the good agreement between the numerical model and the experimental procedure.

Following the successful application of the numerical model to a simple experimental procedure, the model was modified to account for more complex chemical reactivity, where the rate constant is incorporated into the calculation of the concentration distribution. This model was then applied to the kinetic study of

(38) Hanley, Q. S.; Subramaniam, V.; Arndt-Jovin, D. J. *Cytometry* **2001**, *43*, 248–260.

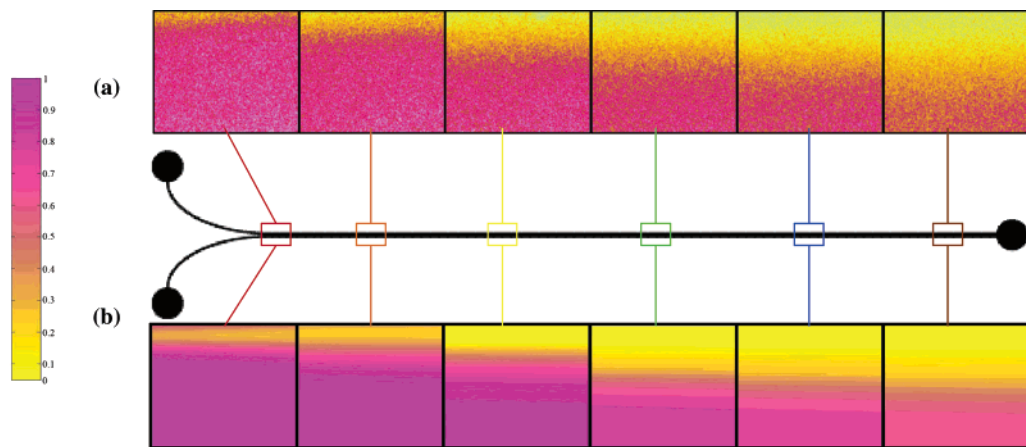


Figure 12. Normalized lifetime maps for (a) experimental and (b) simulated data for the reaction between 2-aminoacridone and benzoyl chloride. The experimental error in each pixel was estimated using the standard deviation of the data in a row along the channel and was found to be $\pm 5\%$. Note the error in a single pixel is much larger than the error for points in the profile across the channel as to produce one point in the profile plots 250 pixels along the channel are averaged.

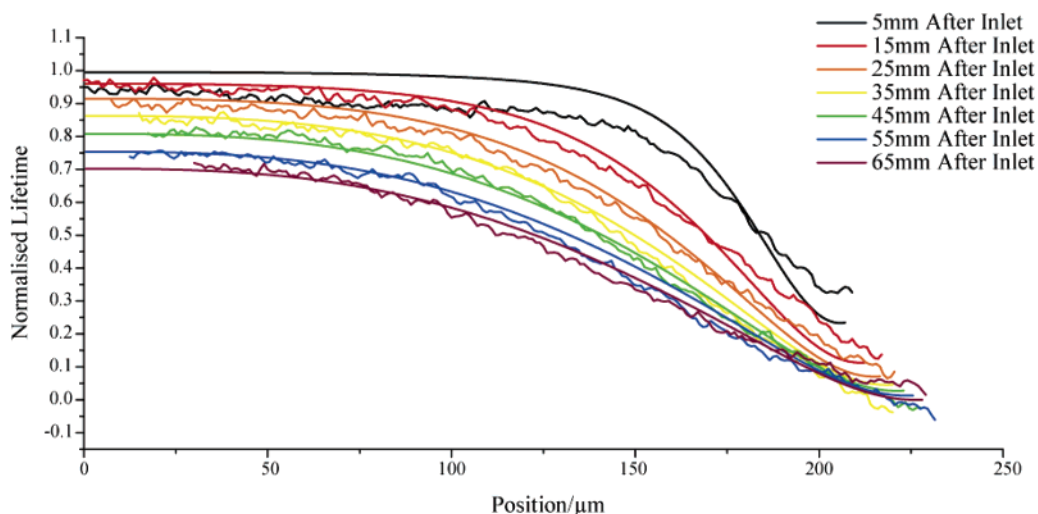


Figure 13. Comparison of experimental and simulated normalized lifetime profiles for the reaction between 2-aminoacridone and benzoyl chloride.

the second-order reaction between 2-aminoacridone and benzoyl chloride.

The amide bond-forming reaction between an acid chloride and amine has been well studied for a variety of aliphatic and aromatic compounds.^{39,40} The reaction is known to be second order overall, first order with respect to each of the reactants; the proposed mechanism is shown in Figure 10. Previously published results for similar compounds have reported a bimolecular rate constant of $1.6 \times 10^4 \text{ mol}^{-1} \text{ dm}^3 \text{ s}^{-1}$ for the model reaction between benzoyl chloride and aniline.³⁹

As stated previously, the reaction is expected to be a second-order reaction following the scheme and rate law shown below:



The required modifications to the boundary conditions have been described previously.²⁵

The parameters used are as follows: $N_K = 6500 - 10\,000$, $N_J = 800$, $N_I = 60$, $h_2 = 0.025 \text{ cm}$, $d_d = 0.05 \text{ cm}$, $x_1 = 7 \text{ cm}$, $v_f = 0.003 \text{ cm}^3 \text{ s}^{-1}$, $D_{2-AA} = 2.96 \times 10^{-5} \text{ cm}^2 \text{ s}^{-1}$, and $D_{BC} = 4.2 \times 10^{-5} \text{ cm}^2 \text{ s}^{-1}$. The diffusion coefficients for 2-aminoacridone and benzoyl chloride were estimated using the Wilkie Chang equation.⁴¹

In order to compare experimental and simulated lifetimes, both were normalized; the experimental results were normalized by allocating the lifetime when no reaction had occurred a value of 1 and the minimum lifetime obtained by the end of the channel a value of 0. The simulated data were normalized so that when the concentration of species C was 0 and the concentration of species A was 1 the normalized value was 1, the maximum value of C at the end of the channel was given a normalized value of 0.

As described previously, the simulated lifetime images are produced by averaging the lifetime over the imaging section to match the wide-field image obtained. A 2 mm section of the channel is shown in each image, and the corresponding profile represents the average lifetime over this image.

(39) King, I. F.; Rathore, R.; Lam, J. Y. L.; Guo, Z. R.; Klassen, D. F. *J. Am. Chem. Soc.* **1992**, *114*, 3028–3033.

(40) Alberghina, G.; Arcoria, A.; Fisichella, S. *J. Org. Chem.* **1978**, *43* (6), 1122–1125.

(41) Welty, J. R.; Wicks, C. E.; Wilson, R. E.; Rorrer, G. *Fundamentals of Momentum, Heat and Mass Transfer*; John Wiley & Sons: New York, 2000; pp 439–446.

In order to calculate a rate constant for the reaction, a series of simulations with rate constant varying from 1×10^1 to 1×10^6 $\text{dm}^3 \text{mol}^{-1} \text{s}^{-1}$ were run and the normalized lifetime profiles are shown in Figure 11.

The simulations demonstrate that the system is sensitive to a change in rate constant of 5 orders of magnitude for the simulated geometry, and it is possible to tune this region of sensitivity by changing the volume flow rate.

A 2.3×10^{-4} mol dm^{-3} solution of 2-aminoacridone was introduced at one inlet and a 2.3×10^{-2} mol dm^{-3} solution of benzoyl chloride introduced at the other with a combined volume flow rate of $0.003 \text{ cm}^3 \text{ s}^{-1}$. The excess of benzoyl chloride was used to ensure significant reaction occurred within the microchannel; the concentration of 2-aminoacridone could not be increased as this caused the product to exceed its solubility and a solid product was formed in the microchannel. A solid in the channel not only disturbs the flow profile but also affects the measurement of the lifetime.

The experimental lifetime images obtained are shown in Figure 12. Figure 11 shows that a rate constant of $1 \times 10^3 \text{ dm}^3 \text{mol}^{-1} \text{s}^{-1}$ or less results in a series of profiles that do not intersect; rate constants above $1 \times 10^4 \text{ dm}^3 \text{mol}^{-1} \text{s}^{-1}$ result in the profiles crossing prior to reaching a minimum. Close inspection of the experimental profiles in Figure 12 reveals that the profiles nearer the inlet remain separated but further downstream some of profiles do cross over, indicating a rate constant with a value between 1×10^3 and $1 \times 10^4 \text{ dm}^3 \text{mol}^{-1} \text{s}^{-1}$. Further simulations with rate constants in this region were completed and identified a bimolecular rate constant for the reaction of $2 \times 10^3 \text{ dm}^3 \text{mol}^{-1} \text{s}^{-1}$. A

comparison of the experimental and simulated normalized lifetime profiles is shown in Figure 13.

CONCLUSION

We have presented a method for the quantitative kinetic analysis of reaction processes occurring within a microfluidic device using numerical simulations. A three-dimensional finite difference model was developed to account for mass transport and reaction kinetics within the microchannel. This model was then used to extract a rate constant from experimental data obtained using fluorescence lifetime imaging.

The numerical method was first applied to previously published experimental results for the iodide ion quenching of Rhodamine 6G. Good agreement between the simulated and experimental data was observed. The method was then applied to a chemical reaction between 2-aminoacridone and benzoyl chloride. Numerical simulations demonstrated that the lifetime profiles were sensitive to the applied rate constant; altering experimental conditions such as volume flow rate or channel dimensions could change this region of sensitivity. Comparison of simulated and experimental data identified a second-order rate constant of $2 \times 10^3 \text{ dm}^3 \text{mol}^{-1} \text{s}^{-1}$.

ACKNOWLEDGMENT

This work was funded by Syngenta Ltd. and the EPSRC. C.F.K. thanks the Leverhulme Trust for personal sponsorship.

Received for review January 9, 2007. Accepted March 19, 2007.

AC070045J